VoR of this paper: Phys. Status Solidi A, 211: 251–259 (2014). doi:10.1002/pssa.201330085

Link to the VoR: http://dx.doi.org/10.1002/pssa.201330085

VoR of this paper: Phys. Status Solidi A, 211: 251–259 (2014). doi:10.1002/pssa.201330085

Link to the VoR: http://dx.doi.org/10.1002/pssa.201330085

CVD precursors for transition metal oxides nanostructures: molecular properties, surface behavior and temperature effects.

Gloria Tabacchi [*,1], Ettore Fois[1], Davide Barreca[2], and Alberto Gasparotto[3]

[1] Department of Science and High Technology, Insubria University and INSTM, via Lucini 3, I-22100, Como, Italy
[2] CNR-IENI and INSTM - Department of Chemistry and Padova University, I-35131, Padova, Italy
[3] Department of Chemistry, Padova University and INSTM, I-35131, Padova, Italy

Keywords Surface chemistry, density functional calculations, molecular dynamics, chemical vapor deposition, transition metals

* Corresponding author: e-mail gloria.tabacchi@uninsubria.it, Phone: +00 39 031 238 6614, Fax: +00 39 031 238 6630

Integrated analyses on a series of β-diketonate-diamine transition metal complexes (M = Fe, Co, Cu, Zn), highlight the metal center influence on molecular physico-chemical properties and provide understanding of the favorable behavior of these complexes as metal sources in the CVD growth of metal/metal oxides nanomaterials. The Zn complex, which shows the most symmetric coordination environment in the gas phase, is activated in contact with the heated CVD growth surface model. First-principles simulations evidenced surface-induced rolling motion of the Zn precursor in the 363-750 K range, suggesting the relevance of vibrationally excited molecular rolling as activation pathway in high temperature surface chemistry.

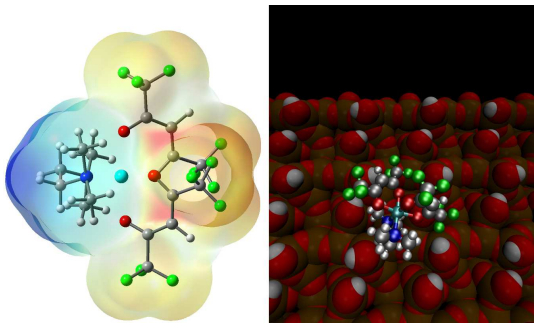

Molecular properties (left) and hot-surface behavior (right) of the $Zn(hfa)_2TMEDA$ CVD precursor.

1 Introduction The bottom-up fabrication of functional nanomaterials through the decomposition of molecular precursors on heated surfaces is a technologically strategic process at the basis of a plethora of applications. In this context, Chemical Vapor Deposition (CVD) routes, in which the source compounds are initially brought into the vapour phase, are well-established and very versatile approaches to control the nucleation/growth of specific nanomaterials [1]. A careful choice of the operating conditions, *e.g.*, substrate temperature and nature, reaction atmosphere, pressure and flow rates, molecular precursor enables the obtainment of nanosystems with prescribed composition, morphology and spatial organization [2]. However, in spite of such progresses, the microscopic-level details of the processes are still mostly obscure. In this regard, computational modelling combined with experimental studies could be of key importance to achieve such molecular-level insight, promoting further progresses in this strategic research area [3].

The precursor chemistry lies at the origin of the properties of the resulting CVD materials. Prediction of the chemico/physical behavior of source molecules could help in developing novel precursors, characterized by high volatility, intact vaporization and clean decomposition into the target (nano)materials [4,5]. Moreover, knowledge of precursor molecular properties is a crucial step to understand how the precursor interacts with the growth surface, as well as with other gaseous species, under the operating CVD conditions [3]. In this context, modeling approaches are playing an increasingly important role, but further progress is needed in order to gain fundamental knowledge of the basic chemistry of CVD processes. [3, 6-9]
A broad variety of transition metal/metal-oxides nanomaterials can be developed starting from the so-called second generation precursors. These are, in general, stable complexes with shelf-life and mass transport properties superior to conventional coordination compounds [10], thanks to the full saturation of the metal coordination

sphere by sterically demanding ligands. In this broad scenario, an attractive family of compounds are the β-diketonate-diamine complexes with general formula $M(hfa)_2TMEDA$ (hfa=1,1,1,5,5,5 - hexafluoro - 2,4 – pentanedionate; TMEDA=N,N,N',N' - tetramethylethylenediamine), where M is a divalent first-row transition metal (*e.g.*, Fe, Co, Cu, Zn) [11-15]. These precursors possess very favourable properties for the deposition of the corresponding metal/metal oxide nanomaterials. For instance, ZnO nanoarchitectures may be obtained starting from the Zn precursor [11], whereas both CuO and Cu_2O oxides can be fabricated from $Cu(hfa)_2TMEDA$ through a proper selection of the process parameters [16]. Integrated experimental-computational analyses have clarified the metal-ligands bonding [13] and unraveled the gas-phase fragmentation mechanism of $Cu(hfa)_2TMEDA$ [17]. Further studies on the Co [18] and Fe [14, 15] homologues have revealed that properties and reactivity of this kind of precursors are significantly influenced by the metal center M. In fact, despite all $M(hfa)_2TMEDA$ complexes present a *pseudo*-octahedral structure with a MO_4N_2 core [13-15, 18], they show structural differences accompanied by diverse gas phase behaviors. For instance, the first step of the $Fe(hfa)_2TMEDA$ fragmentation is the loss of the neutral TMEDA ligand [15], whereas release of a negatively charged diketonate hfa occurs for the Cu compound [13, 17]. Furthermore, by studying the interactions of the Cu precursor with the heated substrate, a new type of surface behavior, defined as fast rolling diffusion on the hot surface (T=750 K) [19], was evidenced. This molecular cartwheeling motion, also characterized by significant vibrational excitation of metal-ligand bonds, might promote high-energy collisions on the growth surface, which could, in turn, activate decomposition processes. Nevertheless, in spite of such information, the behavior of CVD molecular precursors on growth substrates still remains a largely unexplored issue which certainly deserves further attention. For example, it would be relevant to establish whether the molecular tumbling observed for $Cu(hfa)_2TMEDA$ [19] could be a general aspect of high-temperature surface chemistry. A first step towards this broader perspective picture is undoubtedly the investigation of the behavior presented by analogous CVD precursors under the same experimental conditions.

In an attempt to gain further insights on the interrelations between the chemical behavior and the metal center nature, the present work reports a comprehensive investigation on $M(hfa)_2TMEDA$ precursors, where novel results on molecular and surface properties of the Zn homologue, $Zn(hfa)_2TMEDA$, will be presented and discussed through comparison with the other complexes of the family.

In particular, a joint experimental-theoretical approach is adopted for the Zn precursor characterization, whereas the behavior of the Zn complex in contact with the hot surface of a CVD substrate is modelled and compared with the case of $Cu(hfa)_2TMEDA$ [19]. Since the adopted temperature plays a key role in determining behavior, properties and reactivity of the precursor/surface system [3], the behavior of the target Zn precursor on the model growth surface is investigated at different temperature conditions.

2 Materials and methods

2.1 Experimental $Zn(hfa)_2TMEDA$ was synthesized according to previously reported procedures [11,20]. FT-IR analyses were performed on KBr pellets in transmittance mode by means of a Thermo-Nicolet Nexus 860 spectrophotometer, using a spectral resolution of 4 cm^{-1}.

2.2 Computational Density Functional Theory (DFT) calculations on the $Zn(hfa)_2TMEDA$ complex (spin multiplicity = 1) were performed by the Gaussian 09 (G09) code [21]. Optimized structures and vibrational (harmonic) frequencies were calculated with the M06 hybrid functional [22]. An ECP10-MDF pseudopotential [23] with the aug-cc-pVDZ-PP basis set was adopted for Zn [24]. Full double zeta plus diffuse and polarization functions basis sets (D95+*) were adopted for the ligand atoms [25]. X-ray coordinates [20] were used as guess positions in the optimizations, yielding structures with positive harmonic frequencies. For the comparison of the calculated vibrational spectrum with experimental IR data, following a standard practice, a shift factor of 0.97 was applied to calculated wavenumbers [26]. $Zn(hfa)_2TMEDA$ geometry was also optimized by using the B3LYP and PBE functionals, providing close results (see Table 1).

Binding energies of the TMEDA and hfa ligands in $Zn(hfa)_2TMEDA$ were calculated at the M06/D95+* theory level. The counterpoise correction for basis set superposition errors was applied. Structural relaxation of the hfa and TMEDA fragments was kept into account.

The temperature effects on the $Zn(hfa)_2TMEDA$ complex were studied by First Principles Molecular Dynamics (FPMD) [27, 28] simulations with the CPMD code [29]. The Perdew–Burke–Ernzerhof (PBE) functional [30] was adopted, with plane wave (PW) basis sets and ultrasoft pseudopotentials [31] for all atoms. For the isolated complex, a cubic box of 1.69 nm length with PW cut-off of 25 and 200 Ry for orbital expansion and electronic density representation, respectively, was adopted. Benchmark tests at higher cut-off values were performed as well. The PW/PBE minimum energy structure was calculated by a geometry optimization. Such a structure, which was very close to the optimized ones computed with localised basis sets (see Table 1), was used as starting configuration for a 12 ps-long simulation at T=340 K, *i.e.* slightly above the complex sublimation temperature (T=333 K). A time step of 0.121 fs was used for trajectory integration, with an inertia parameter of 500 atomic units (au) for the electronic coefficients [28].

The behavior of $Zn(hfa)_2TMEDA$ on the CVD growth surface was simulated with DFT, periodic boundary conditions and plane waves (PW) basis sets. Under the experimental conditions adopted in CVD experiments (precursor vaporization temperature = 333 K, O_2+H_2O atmosphere,

Si(100) support heated in the 523-773 K temperature range) [11], the exposed surface is hydroxylated SiO_2 [32]. The model adopted to simulate the growth surface is therefore a 1 nm thick periodically repeated slab (stoichiometry: $Si_{36}O_{72}\cdot 8H_2O$) of 1.69 × 1.69 nm^2 area, with a concentration of 2.8 surface silanol groups per nm^2. Such a model, previously adopted for the Cu homologue precursor [19], has also provided adequate descriptions for other surface phenomena [33,34]. A 1.69×1.69×2.6 nm^3 simulation box was used for the ($Zn(hfa)_2$TMEDA + surface) model system, composed by 185 atoms. The starting configuration was built by using $Zn(hfa)_2$TMEDA coordinates taken from random configurations sampled along the FPMD trajectory of the isolated complex, and positioning the precursor molecule on the model surface with a random orientation. FPMD simulations were performed with the CPMD code [29]. Ultra-soft pseudopotentials [31] were used for Zn, F, O, N, C, H, whereas a norm-conserving pseudopotential was adopted for Si [35, 36]. This electronic structure calculation scheme provides an adequate description of large sized inorganic-organic systems [19, 37-40] As for the 340 K isolated precursor simulation, the PBE density functional [30] was adopted, along with the same PW cutoff values and computational scheme for trajectory integration.

Data were collected from three production runs (MD1, MD2, MD3) of 20 ps each in the canonical ensemble, performed by selecting target temperatures of 363, 500 and 750 K, respectively. Nose–Hoover thermostats [41] and 6 ps equilibration time were adopted in all simulations.

Geometry optimizations of the ($Zn(hfa)_2$TMEDA + surface) system were performed on different configurations sampled along the trajectories. Among the optimized structures, the lowest energy one provided the $Zn(hfa)_2$TMEDA physisorption geometry. The complex-surface binding energy BE was calculated by the formula:

$$BE = E(complex+surface) - E(complex) - E(surface) \quad (1)$$

where E(complex+surface) is the energy of physisorbed $Zn(hfa)_2$TMEDA, while E(complex) and E(surf) are the energies of the isolated complex and substrate slab, respectively, optimized in the simulation box adopted for the overall system. All geometry optimizations with PW basis were performed by adopting a quasi-Newton algorithm [28] and a convergence criterion of 10^{-4} au for the maximum force per atom.

Calculations were performed at the Centro di Calcolo Scientifico of Insubria University and at the CINECA Italian Supercomputing Center (Bologna).

3 Results and discussion

3.1 Molecular properties of the precursor

3.1.1 $Zn(hfa)_2$TMEDA structure and stability

The minimum energy structure of the $Zn(hfa)_2$TMEDA complex, shown in Fig. 1, is characterized by a C_2 symmetry with the 2-fold axis bisecting the diamine ligand, and a six-fold Zn coordination.

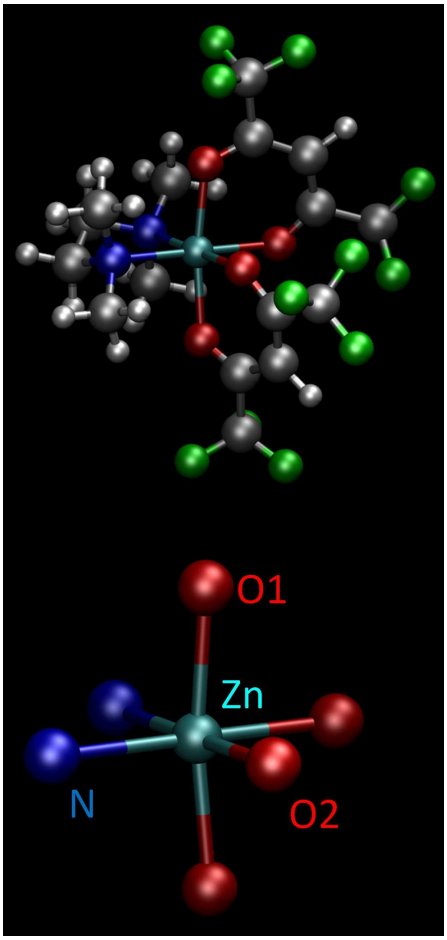

Figure 1 Top: Minimum energy structure of $Zn(hfa)_2$TMEDA (M06/D95+* level). Bottom: enlarged view of the *pseudo*-octahedral Zn coordination environment. Color codes: Zn: cyan, F: green, O: red, N: blue, C: grey, H: white.

As in the homologous Co [18], Fe [14] and Cu [13] complexes, the two β-diketonate and diamine ligands are bound to the metal center according to a distorted octahedral geometry. Bond distances and angles of the ZnO_4N_2 coordination octahedron, calculated for the isolated Zn complex at different theory levels, are reported in Table 1 and compared with the corresponding X-ray values taken from Ref. [20].

Calculated bond angles evidence modest distortions of ZnO_4N_2 from a perfect octahedral geometry. Bond lengths values indicate that the Zn coordination environment is actually rather symmetrical, with close values of the Zn-O1 and Zn-O2 distances and slightly longer Zn-N bonds. All the tested density functional approximations successfully reproduce these general features. In particular, the results obtained with a pure DFT functional and PW basis (PBE/PW) agree to a good extent with higher level data

calculated with hybrid functionals and Gaussian basis sets. Such an agreement is of relevance in view of $Zn(hfa)_2TMEDA$ modelling on the growth surface, accessible only through the former approach. The results on precursor molecular properties presented hereafter will refer to the M06 functional, unless otherwise stated.

Table 1 Geometrical parameters of $Zn(hfa)_2TMEDA$. Atom numbering as in Fig. 1.

distance (Å)	M06	B3LYP	PBE	PBE/PW	Exp*
Zn-O1	2.079	2.100	2.110	2.121	2.102
Zn-O2	2.095	2.112	2.114	2.132	2.126
Zn-N	2.159	2.283	2.220	2.233	2.145
angle (°)					
O1-Zn-O1	171.1	170.6	171.3	171.2	173.6
O2-Zn-N	178.4	176.5	176.9	176.5	174.8
O1-Zn-N	92.8	93.5	93.0	93.2	89.8
	93.8	93.5	93.4	93.3	94.4
O1-Zn-O2	86.4	85.6	86.8	85.9	85.1
	87.2	87.8	87.0	87.9	89.5

* From Ref. [20].

Beside relevant information on structure and metal-ligand bonding of this precursor, computational results also provide valuable insights on its stability. The binding energies of the TMEDA and hfa ligands in the $Zn(hfa)_2TMEDA$ complex were calculated from energy differences related to the decomposition pathways sketched in Eq. (2) and (3), respectively.

$$Zn(hfa)_2TMEDA \rightarrow Zn(hfa)_2 + TMEDA \quad (2)$$

$$Zn(hfa)_2TMEDA \rightarrow Zn(hfa)TMEDA + hfa \quad (3)$$

In both cases, the loss of one ligand desaturates the Zn coordination sphere and, in the resulting fragment, the metal center exhibits a tetrahedral coordination. Loss of the diamine ligand is thermodynamically favoured because of the lower TMEDA binding energy (40.8 kcal × mol^{-1}) with respect to the hfa one (115.8 kcal × mol^{-1}). Nevertheless, both values are high enough to ensure a precursor vaporization free from undesired side-reactions. Under such conditions, full saturation of the Zn coordination sphere should be maintained and detrimental gas phase precursor degradation processes should not be significant. Nonetheless, precursor decomposition might be triggered by high-energy activation pathways occurring upon interaction with the heated CVD growth surface [19].

Table 2 Zn-L bond lengths in $Zn(hfa)_2TMEDA$ from FPMD. Atom numbering as in Fig. 1.

*distance (Å)	
Zn-O1	2.15 (0.10)
	2.16 (0.11)
Zn-O2	2.16 (0.12)
	2.15 (0.11)
Zn-N	2.27 (0.11)
	2.30 (0.12)

* Data calculated at the PBE/PW level. Computed standard deviations (in parentheses) provide an estimation of thermal oscillation amplitudes.

In line with the above results, the compound stability under CVD vaporization conditions is also suggested by a FPMD simulation (PBE/PW level) at 340 K (*i.e.* slightly above the experimentally adopted sublimation temperature, 333 K [11]). As indicated by the calculated average Zn-ligand distances and standard deviations (Table 2), at 340 K the $Zn(hfa)_2TMEDA$ octahedral geometry is preserved. Moreover, all Zn-ligand bonds exhibit only modest elongations with respect to the 0 K minimum energy structure (Table 1) and rather small thermal fluctuations.

3.1.2 $Zn(hfa)_2TMEDA$ vibrational properties The experimental and calculated IR spectra of the complex are superimposed in Fig. 2. Since $Zn(hfa)_2TMEDA$ spectrum is similar to those observed for Fe, Co, Cu homologues, we refer to such studies for a thorough interpretation in terms of band assignment [13,14,18] and focus herein only on the main vibrational features. It should be highlighted that the calculated vibrational spectrum is obtained from the minimum energy structure harmonic frequencies and refers to an isolated precursor molecule, thus neglecting interactions with surrounding molecules in the $Zn(hfa)_2TMEDA$ crystal, which, on the contrary, affect the experimental spectrum. On this basis, agreement between the red and black curves in Fig. 2 can be considered satisfactory, allowing thus the elucidation of spectral features. For sake of clarity, in the relative discussion we will adopt experimental wavenumbers unless otherwise specified.

The highest wavenumber signal at 3141 cm^{-1} and the 3022-2813 cm^{-1} multipeak pattern are due to C-H stretching modes of the hfa and TMEDA ligands, respectively. The intense bands at 1669 and 1651 cm^{-1} arise from hfa carbonyl groups, whereas hfa C=C stretching/C-H bending modes and TMEDA CH_2/CH_3 deformation are associated to the 1554-1385 cm^{-1} signals. The 1346 cm^{-1} peak is ascribed to C=C and C-CF_3 stretching modes, whereas bands at 1261, 1197 and 1144 cm^{-1} can be attributed to C-H bending and C-CF_3/C-F stretching. C-C / C-N stretching bands appear at lower wavenumbers (934-1105 cm^{-1}). Finally, stretching modes related to metal-ligand bonds are responsible for signals in the 448-584 cm^{-1} range. In particular, the 584 cm^{-1} band arises solely from Zn-O stretching, while the 494 cm^{-1} peak should essentially be attribut-

ed to the Zn-N one. Interestingly, vibrational analysis indicates that the other bands in such interval arise from combinations of the Zn-O1, Zn-O2 and Zn-N stretching modes, involving the whole Zn coordination environment. The presence of such collective metal-ligand vibrations arises from the absence of remarkable asymmetries in the ZnO_4N_2 metal-ligand bond distances, as discussed in section 3.1.1.

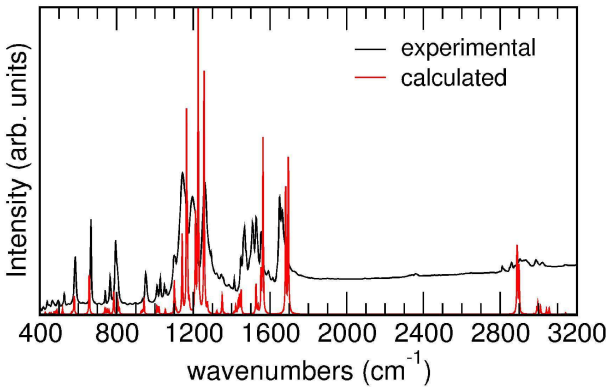

Figure 2 Comparison of experimental and calculated IR spectra of $Zn(hfa)_2TMEDA$. A 2 cm^{-1} Gaussian broadening and a 0.97 scaling factor was applied to calculated wavenumbers.

3.1.3 General features of $M(hfa)_2TMEDA$ precursors Besides relevant insight on $Zn(hfa)_2TMEDA$ properties, the above presented results, upon comparison with those obtained for the Fe, Co and Cu homologues, could help elucidating general aspects of the chemistry of this series of CVD precursors. Indeed, a deeper molecular-level understanding of $M(hfa)_2TMEDA$ chemical behavior could be gathered from the analysis of similarities and differences in precursor properties as a function of the metal center (Table 3).

Table 3 Spin multiplicity, metal-ligand bond lengths (Å) and molecular dipole moments μ (D) in $M(hfa)_2TMEDA$ (M = Fe, Co, Cu, Zn).

*	Fe**	Co	Cu	Zn
spin	quintet	quartet	doublet	singlet
M-O1	2.041	2.050	2.287	2.079
M-O2	2.091	2.066	1.977	2.095
M-N	2.230	2.178	2.062	2.159
μ	7.62	7.38	8.99	8.14

* All data are calculated at the M06/D95+* level.
** From Ref. [14].

First, the four $M(hfa)_2TMEDA$ precursors here considered have different spin states, and, as a consequence, may show appreciably different behavior both in the gas phase and under CVD conditions [13, 15, 18].

Since metal-ligand bonds strongly affect precursor reactivity, valuable insight could be obtained by comparing M-L bond lengths within the $M(hfa)_2TMEDA$ series. As observed in Table 3, both Fe and Cu complexes show significant distortions from an ideal octahedron. However, whereas the apical Fe-O1 distances are shorter than the equatorial Fe-O2 bonds, the Cu-O1 distances are much longer than the Cu-O2 ones. This difference in the metal-oxygen bond lengths on apical and equatorial positions for Fe and Cu precursors is related to diamine *trans* effects and Jahn-Teller distortion, respectively [13, 15]. On the other hand, the Co and Zn precursor geometries are characterized by similar M-O1 and M-O2 distances and slightly larger M-N separation, and, hence, by more regular MO_4N_2 geometries. Along this series of precursors, the shortest and longest M-N bonds are found, respectively, in the Cu and Fe complex, whereas $Cu(hfa)_2TMEDA$ contains simultaneously the shortest and longest M-O distances. Such data are also in line with the trends of the calculated M-O and M-N stretching frequencies along the $M(hfa)_2TMEDA$ series (Table 4). As an example, the highest and lowest ν(M-N) are found for the Cu and Fe homologues, respectively. In general, these precursors present complex metal-ligand vibrational modes, characterized by different M-O/M-N stretching combinations. Nevertheless, only in the case of the most symmetric compound $Zn(hfa)_2TMEDA$ such combinations involve the whole coordination environment and can be considered collective modes of the ZnO_4N_2 octahedron.

Table 4 Calculated metal-ligand stretching frequencies in $M(hfa)_2TMEDA$ (M = Fe, Co, Cu, Zn).

*ν (cm^{-1})	Fe**	Co	Cu	Zn
M-O	499 534 584-600	475 497 590-598	374-380 585-601	464 588-596
M-O/M-N	473 498	479 496	465 500 509	472 481
M-N	461 490	468 502	514	503

* Frequency values (not scaled) calculated at the M06/D95+* level.
** From Ref. [14]

Besides analogies in structural and spectroscopic properties, $M(hfa)_2TMEDA$ complexes also show similar electrostatic potential maps with negative and positive regions associated to the hfa and TMEDA ligands respectively, as clearly evidenced in Fig. 3 for the Zn complex. As a consequence, they are all characterized by high values of the molecular dipole moment, which is oriented along the 2-fold axis bisecting the diamine ligand. An inspection of dipole moments and M-N bond lengths/stretching frequencies (Tables 3-4) reveals an increase of dipole moments proportionally to M-N bond strength. This phenomenon can be rationalized by considering that, since TMEDA acts as an electron donor towards the metal center, shorter M-N distances imply a higher ligand charge depletion, producing, in turn, a higher dipole moment.

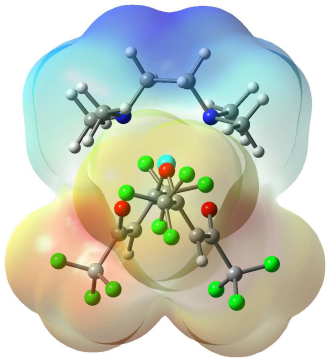

Figure 3 Electrostatic potential map of the $Zn(hfa)_2TMEDA$ complex. Areas of high (positive) potential (in blue) are characterized by a relative absence of electrons, whereas areas of low (negative) potential (in red) are characterized by a relative abundance of electrons. Intermediary colors represent intermediary electrostatic potential values. $Zn(hfa)_2TMEDA$ atom color codes as in Fig.1.

This analysis of $M(hfa)_2TMEDA$ precursor family indicates that, whereas the Cu complex shows the largest asymmetry in M–O distances, the Zn one is characterized by the most symmetric coordination environment. Such structural differences, accompanied by the corresponding differences in vibrational and charge distribution properties, could have relevant consequences on the precursor reactivity. Indeed, in the case of $Cu(hfa)_2TMEDA$, the interactions of O2 with the metal centre are much stronger compared to O1, suggesting an easier cleavage of the latter bond and therefore an easier loss of the hfa ligand with respect to the TMEDA one. This was actually observed in the precursor gas phase Mass Spectrometry (MS) fragmentation [13, 17]. Moreover, the presence of a weak Cu-O contact in the complex appreciably affected also its surface behavior, characterized by large temperature-induced fluctuations of this labile M-L bond [19]. For these reasons, it is of utmost importance to investigate $Zn(hfa)_2TMEDA$ on the heated CVD growth substrate and compare the surface behavior of these two complexes.

3.2 $Zn(hfa)_2TMEDA$ behavior on the CVD growth surface As mentioned in the Introduction, due to the fully saturated environment of the metal center in $M(hfa)_2TMEDA$, it is difficult to figure out possible reactive pathways for such complexes on the growth surface. The first ligand loss should, however, represent a key step in the precursor decomposition, since the coordination sphere desaturation may allow the metal centre to come into direct contact with the substrate surface atoms. The high binding energies calculated for hfa and TMEDA ligands in the isolated $Zn(hfa)_2TMEDA$ molecule (see section 3.1.1) highlight a considerable thermodynamic stability of this precursor and suggest that activation processes, promoted by high temperature conditions/interactions with the growth surface, should be necessary to cleave metal-ligand bonds.

In this context, it is worth recalling that water acts as a catalyst for precursor decomposition both in the gas phase and on the substrate surface, where water molecules are dissociatively chemisorbed forming surface silanol groups that favor the precursor's anchoring. Water effects were not considered in the homogeneous gas phase calculations on $M(hfa)_2TMEDA$, which were designed to provide a hint on the precursors' thermal behaviour. Conversely, in order to gather a proper description of the heterogeneous phase processes, in the precursor/substrate system water was modelled as already chemisorbed on the growth surface, in the form of silanol groups.

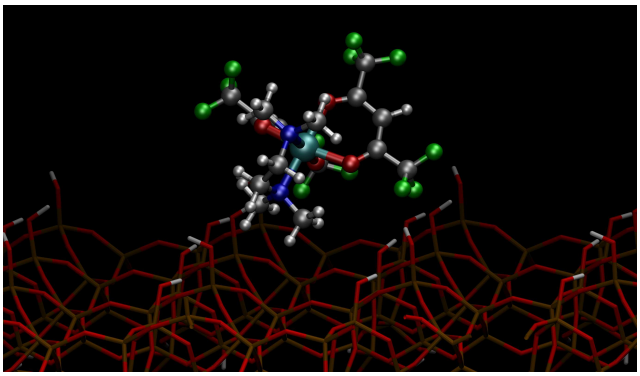

Figure 4 Graphical representation of the minimum energy structure of the $Zn(hfa)_2TMEDA$/hydroxylated silica slab system. Slab color codes: Si: brown, O: red, H: white. $Zn(hfa)_2TMEDA$ atom color codes as in Fig.1.

The minimum energy structure of the ($Zn(hfa)_2TMEDA$+surface) system, shown in Figure 4, closely resembles the physisorption geometry calculated for the Cu homologous [19]. In fact, the molecule is in contact with the surface silanol oxygens through the TMEDA methyl and methylene groups, whereas hfa CF_3 moieties point away from the surface. Such an arrangement can be understood on the basis of the $Zn(hfa)_2TMEDA$ electrostatic potential map (Figure 3): the molecule interacts with surface oxygens *via* its most electron-poor regions. Bond distances of the adsorbed Zn complex reported in Table 5 evidence that, when in contact with the surface, the C_2 symmetry characterizing the gas-phase molecular geometry is no longer preserved. In particular, among the Zn-O1, Zn-O2, Zn-N pairs, the bond closer to the surface is also the one showing the larger deviations with respect to the gas-phase minimum energy structure (see also Table 1). These findings, well in line with previous ones for the Cu precursor [19], confirm that complex-surface interactions distort the metal coordination environment. Even in the present case, in the physisorption geometry the distance of the metal center from the closest surface oxygen is well above 5 Å (Table 5), still too long for a direct interaction with surface atoms. On the other hand, the calculated

$Zn(hfa)_2TMEDA$ physisorption energy, 5.6 kcal/mol, is small enough to ensure that, under the temperature conditions normally used in CVD experiments, thermal activation processes should occur with a high probability [3, 19].

Table 5 Average Zn-L bond lengths (Å) in $Zn(hfa)_2TMEDA$

*	OPT	MD1	MD2	MD3
T (K)	0	363	500	750
Zn-O1	2.136	2.18 (0.17)	2.24 (0.25)	3.17 (0.99)
	2.142	2.16 (0.14)	2.14 (0.12)	2.13 (0.15)
Zn-O2	2.131	2.18 (0.14)	2.22 (0.22)	2.08 (0.17)
	2.143	2.17 (0.14)	2.20 (0.17)	2.18 (0.20)
Zn-N	2.244	2.28 (0.13)	2.32 (0.18)	2.43 (0.47)
	2.203	2.29 (0.13)	2.28 (0.13)	2.68 (0.85)
**Closest Zn-O_{surf}	5.428	5.734 (3.418)	7.137 (4.972)	6.167 (4.877)

* All data are calculated at the PBE/PW level.
** For MD1,MD2,MD3, average values of the distance of Zn from the closest surface oxygen atom are reported. The values in parentheses refer to the minimum distance sampled along each trajectory.

These observations lead now to consider the actual behavior of $Zn(hfa)_2TMEDA$ on the CVD growth surface and its temperature dependency. To this aim, three FPMD trajectories were collected at different temperatures (Table 5). The first one (MD1) was carried out at 363 K, *i.e*. only slightly above the precursor sublimation temperature (333 K), in order to explore molecule-surface interactions in the absence of the harsh conditions typical of a CVD experiment. The other two simulations, MD2 and MD3, were performed at 500 K and 750 K respectively, which approximately correspond to the lower and upper limits of the temperature interval adopted for the CVD process. Remarkably, vibrationally excited rolling motion was detected for the precursor molecule in all the considered temperature range, *i.e.*, not only under standard thermal-CVD operative conditions, but also at significantly lower temperatures, as evidenced by the movie of the T=363 K simulation (see Supporting information). This finding suggests that, besides playing a key role in CVD activation, molecular rolling may be a more general phenomenon characterizing molecule-surface interactions. Support to this hypothesis is also provided by recent studies [42], where small alkene molecules, stimulated either by exotermic surface reactions or by STM electron beams on Si(100), have evidenced a similar behaviour in the 298-443 K range.

By focusing now on the precursor behaviour under CVD conditions, the perturbation of the $Zn(hfa)_2TMEDA$ molecular geometry strongly increases with temperature, as clearly indicated by the obtained Zn-ligand bond lengths (Table 5). In addition, bond distances oscillation observed in the 750 K trajectory are even greater than those detected for the Cu homologue [19]. Even though Zn never comes in direct contact with surface atoms, metal-ligand bonds are transiently broken and the ligands dynamically rearrange around the metal center, as illustrated in Figure 5.

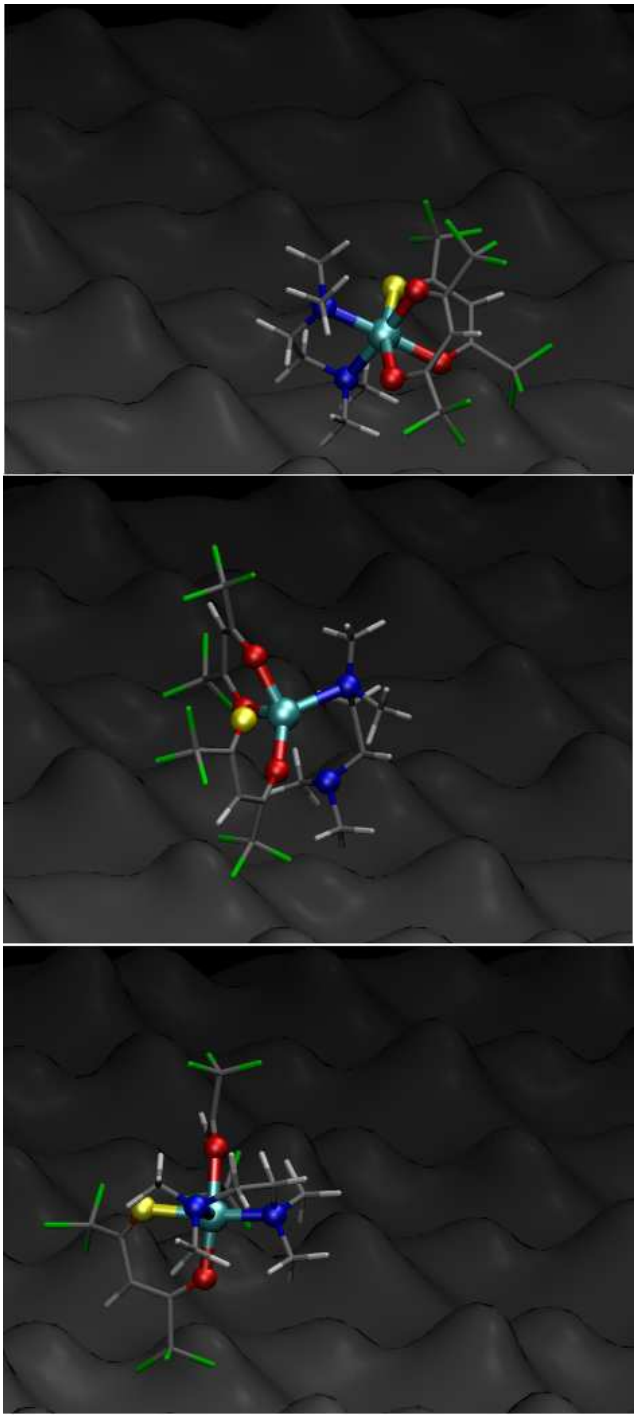

Figure 5 Three snapshots taken from 750 K MD3 trajectory. While the $Zn(hfa)_2TMEDA$ is rolling over the hot surface, an hfa oxygen (yellow), initially in the apical position (top), is moved to the equatorial position (bottom) by a partial ligand detachment (center) Atom color codes as in Fig.1. For clarity, the surface is represented in greyscale.

In particular, the Zn-O1 apical bond length of one hfa ligand (Fig. 5, top) significantly increases during the first simulation stages (0 - 3.6 ps), leading to a partial ligand detachment, which remains bound to Zn by its equatorial oxygen O2. Subsequently, the hfa moiety rotates around the O2-Zn axis, with the complex passing through a distorted tetrahedral geometry (Fig. 5, center), and, after a 180º rotation, the initially apical oxygen bounds again to the metal center, but in an equatorial position (Fig. 5, bottom). Since even the Zn-N distances exhibit similarly large oscillations, it can be concluded that activation of the precursor, induced by interaction with the heated substrate, has been achieved.

As a general consideration, it is to recall that since precursor decomposition timescales are normally much larger than the time scales accessible to FPMD, CVD reactions modelling would require rare events sampling techniques [43-46]. Nevertheless, standard FPMD simulations, beside disclosing the precursor's pre-reactive behaviour on a heated CVD support as evidenced by the above results, could suggest suitable variables for reactive pathways searches, which will be subject of future investigations .

4 Conclusions

Beside relevant insights on the physical chemistry of a series of amenable CVD precursors, the milestones of the present work are the observation of hot-surface induced molecular rolling for $Zn(hfa)_2TMEDA$ and the evidence that this motion occurs at temperature regimes even lower than those normally adopted in CVD experiments. These results strongly support the hypothesis of the general relevance of vibrationally excited molecular rolling in the activation of high temperature surface processes. Finally, the differences between the high temperature behaviors of the Zn and Cu complexes highlighted in the present study might be at the origin of different decomposition pathways of the two precursors on the growth surface, which will be the subject of future investigation. Efforts along this direction are already under way.

Acknowledgements CINECA supercomputing center (Bologna, Italy) is gratefully acknowledged for computing time (ISCRA project 2012 "MONA" HP10BWVM3S). Padova University ex-60% 2012 (n° 60A03-5517), PRAT 2010 (n° CPDA102579) and Insubria University FAR 2012 projects are also acknowledged for financial support. Dr. R. Seraglia (CNR-ISTM, Padova, Italy), Dr. G. Carraro and Dr. C. Maccato (Padova University, Italy), are acknowledged for their precious help in precursor design, synthesis and characterization. Dr M. Oriani (Insubria University, Como, Italy) is acknowledged for technical support in supercomputing.

References

[1] M. L. Hitchman, and A. C. Jones (eds.), Chemical Vapor Deposition: Precursors, Processes and Applications, (Royal Society of Chemistry, Cambridge, UK, 2009).
[2] D. Bekermann, D. Barreca, A. Gasparotto, and C. Maccato, CrystEngComm **14**, 6347 (2012)
[3] G. Tabacchi, E. Fois, D. Barreca, and A. Gasparotto, Int. J. Quantum Chem. DOI 10.1002/qua.24505 (2013).
[4] L. McElwee-White, Dalton Trans. 5367 (2006).
[5] B. Vlaisavljevich, P. Miró, D. Koballa, T. K. Todorova, S. R. Daly, G. S. Girolami, C. J. Cramer, and L. Gagliardi, J. Phys. Chem. C **116**, 23194 (2012).
[6] E. Machado, M. Kaczmarski, B. Braida, P. Ordejón, D. Garg, J. Norman, and H. Cheng, J. Mol. Model. **13**, 861 (2007).
[7] A. Barbato and C. Cavallotti, Phys. Status Solidi B **247**, 2127 (2010).
[8] M. Ceriotti, F. Montalenti, and M. Bernasconi, J. Phys. Condens. Matter **24**, 104002 (2012).
[9] T. Kuwahara, H. Ito, Y. Higuchi, N. Ozawa, and M. Kubo, J. Phys. Chem. C **116**, 12525 (2012).
[10] G. Malandrino and I. L. Fragalà, Coord. Chem. Rev. **250**, 1605 (2006).
[11] D. Barreca, A. P. Ferrucci, A. Gasparotto, C. Maccato, C. Maragno, and E. Tondello, Chem. Vap. Deposition **13**, 618 (2007).
[12] G. Bandoli, D. Barreca, A. Gasparotto, C. Maccato, R. Seraglia, E. Tondello, A. Devi, R. A. Fischer, and M. Winter, Inorg. Chem. **48**, 82 (2009).
[13] G. Bandoli, D. Barreca, A. Gasparotto, R. Seraglia, E. Tondello, A. Devi, R.A. Fischer, M. Winter, E Fois, A. Gamba, and G. Tabacchi, Phys. Chem. Chem. Phys. **11**, 5998 (2009).
[14] D. Barreca, G. Carraro, A. Gasparotto, C. Maccato, R. Seraglia, and G. Tabacchi, Inorg. Chim. Acta **380**, 161 (2012).
[15] D. Barreca, G. Carraro, A. Devi, E. Fois, A. Gasparotto, R. Seraglia, C. Maccato, C. Sada, G. Tabacchi, E. Tondello, A. Venzo, and M. Winter, Dalton Trans. **41**, 149 (2012).
[16] D. Barreca, P. Fornasiero, A. Gasparotto, V. Gombac, C. Maccato, T. Montini, and E. Tondello, ChemSusChem **2**, 230 (2009).
[17] D. Barreca, E. Fois, A. Gasparotto, R. Seraglia, E. Tondello, and G. Tabacchi, Chem. Eur. J. **17**, 10864 (2011).
[18] A. Gasparotto, D. Barreca, A. Devi, R. A. Fischer, E. Fois, A.Gamba, C. Maccato, R. Seraglia, G. Tabacchi, and E. Tondello, ECS Trans. **25**, 549 (2009).
[19] E. Fois, G. Tabacchi, D. Barreca, A. Gasparotto, and E. Tondello, Angew. Chem. Int. Ed. **49**, 1944 (2010).
[20] J. Ni, H. Yan, A. Wang, Y. Yang, C. L. Stern, A. W. Metz, S. Jin, L. Wang, T. J. Marks, J. R. Ireland and C. R. Kannewurf, J. Am. Chem. Soc. **127**, 5613 (2005).
[21] Gaussian 09, Revision D02, M. J. Frisch, G. W. Trucks, H. B. Schlegel, G. E. Scuseria, M. A. Robb, J. R. Cheeseman, G. Scalmani, V. Barone, B. Mennucci, G. A. Petersson, H. Nakatsuji, M. Caricato, X. Li, H. P. Hratchian, A. F. Izmaylov, J. Bloino, G. Zheng, J. L. Sonnenberg, M. Hada, M. Ehara, K. Toyota, R. Fukuda, J. Hasegawa, M. Ishida, T. Nakajima, Y. Honda, O. Kitao, H. Nakai, T. Vreven, J. A. Montgomery, Jr., J. E. Peralta, F. Ogliaro, M. Bearpark, J. J. Heyd, E. Brothers, K. N. Kudin, V. N. Staroverov, R. Kobayashi, J. Normand, K. Raghavachari, A. Rendell, J. C.

1 Burant, S. S. Iyengar, J. Tomasi, M. Cossi, N. Rega, J. M. Millam, M. Klene, J. E. Knox, J. B. Cross, V. Bakken, C. Adamo, J. Jaramillo, R. Gomperts, R. E. Stratmann, O. Yazyev, A. J. Austin, R. Cammi, C. Pomelli, J. W. Ochterski, R. L. Martin, K. Morokuma, V. G. Zakrzewski, G. A. Voth, P. Salvador, J. J. Dannenberg, S. Dapprich, A. D. Daniels, Ö. Farkas, J. B. Foresman, J. V. Ortiz, J. Cioslowski, and D. J. Fox, Gaussian, Inc., Wallingford CT, 2009.

[22] Y. Zhao and D. G. Truhlar, Theor. Chem. Acc. **120**, 215 (2008).

[23] D. Figgen, G. Rauhut, M. Dolg, and H. Stoll, Chem. Phys. **311**, 227 (2005).

[24] K. A. Peterson and C. Puzzarini, Theor. Chem. Acc. **114**, 283 (2005).

[25] T. H. Dunning Jr. and P. J. Hay, Mod. Theor. Chem. **3**, 1 (1976).

[26] A. P. Scott and L. Radom, J. Phys. Chem. **100**, 16502 (1996).

[27] R. Car and M. Parrinello, Phys. Rev. Lett. **55**, 2471 (1985).

[28] D. Marx and J. Hutter, Ab initio Molecular Dynamics (Cambridge Univ. Press, Cambridge, 2009).

[29] CPMD code, MPI für Festkörperforschung: Stuttgart, Germany; IBM Zürich Research Laboratory: Zürich, Switzerland, 1990−2013, www.cpmd.org.

[30] J. P. Perdew, K. Burke, and M. Ernzerhof, Phys. Rev. Lett. **77**, 3865 (1996).

[31] D. Vanderbilt, Phys. Rev. B **41**, 7892 (1990).

[32] P. C. Thüne and J. W. Niemantsverdriet, Surf. Sci. **603**, 1756 (2009).

[33] E. Fois, A. Gamba, G. Tabacchi, S. Coluccia and G. Martra, J. Phys. Chem. B **107**, 10767 (2003).

[34] G. Tabacchi, E. Gianotti, E. Fois, G. Martra, L. Marchese, S. Coluccia, and A. Gamba, J. Phys. Chem. C **111**, 4946 (2007).

[35] D. R. Hamann, M. Schluter, and C. Chiang, Phys. Rev. Lett. **43**, 1494 (1979).

[36] L. Kleinman and D. M. Bylander, Phys. Rev. Lett. **48**, 1425 (1982).

[37] A. Gamba, G. Tabacchi, and E. Fois, J. Phys. Chem A **113**, 15006 (2009).

[38] E. Fois, G. Tabacchi, and G. Calzaferri, J. Phys. Chem. C **114**, 10572 (2010).

[39] E. Fois, G. Tabacchi, and G. Calzaferri, J. Phys. Chem. C **116**, 16748 (2012).

[40] E. Fois, G. Tabacchi, A. Devaux, P. Belser, D. Brühwiler, and G. Calzaferri, Langmuir, DOI 10.1021/la400579w (2013).

[41] S. Nose, J. Chem. Phys. **87**, 511 (1984).

[42] K. R. Harikumar, J. C. Polanyi, A. Zabet-Khosousi, P. Czekala, H. Lin, and W. A. Hofer, Nat. Chem. **3**, 400 (2011).

[43] Henkelman, G.; Jónsson, H. J. Chem. Phys. 2000, 113, 9978-9985.

[44] Iannuzzi, M.; Laio, A.; Parrinello, M. Phys. Rev. Lett. 2003, 90, 238302.

[45] Carter, E.A.; Ciccotti, G.; Hynes, J.T.; Kapral, R. Chem. Phys. Lett. 1989, 156, 472–477.

[46] Sutto, L.; Marsili, S.; Gervasio, F.L. WIREs Comput. Mol. Sci. 2012, 2, 771-779.